The International Conference on Multiphase Systems
Ufa, RUSSIA, June 15-17, 2000
ICMS'2000

The Physics of Boiling at Burnout

*T. G. Theofanous**, *J. P. Tu**, *T.N. Dinh**, *T. Salmassi**, *A.T. Dinh**, *and K. Gasljevic**,

* University of California, Santa Barbara, CA, USA

Abstract.

The basic elements of a new experimental approach for the investigation of burnout in pool boiling are presented. The approach consists of the combined use of ultrathin (nano-scale) heaters and high speed infrared imaging of the heater temperature pattern as a whole, in conjunction with highly detailed control and characterization of heater morphology at the nano and micron scales. It is shown that the burnout phenomenon can be resolved in both space and time. Ultrathin heaters capable of dissipating power levels, at steady-state, of over 1 MW/m^2 are demonstrated. A separation of scales is identified and it is used to transfer the focus of attention from the complexity of the two-phase mixing layer in the vicinity of the heater to a micron-scaled microlayer and nucleation and associated film-disruption processes within it.

1 Introduction

Long after my first fascination with the nucleation and growth of vapor bubbles (Theofanous et al., 1976; 1978) and a brief look at critical heat flux in the interim (Theofanous, 1980), I fell again upon the subject, recently, in connection with an important practical need. I wanted to know the maximum amount of heat I could extract in downward facing boiling from a curved boundary with a radius of curvature ($\sim$ 4 m) many orders of magnitude greater than the characteristic length scale of boiling bubbles. The need arose in trying to demonstrate that a severe (core melt) accident in a nuclear reactor could be stabilized and terminated by submersing the reactor vessel, externally, in a pool of water (Theofanous et al., 1996). The length scale disparity meant that boiling bubbles could not rise, or easily slip along the boundary, before massively coalescing into a macroscopic vapor layer. The stroke of good fortune was not only that we could, in this apparent "film boiling mode", remove up to 600 kW/m^2 with surface superheats typical of nucleate boiling, which assured the success of our accident management scheme (Theofanous et al., 1996; 1997), but also that this peculiar geometry allowed for the first time the detailed observation of the physical processes that define the maximum coolability limits. With my old interests thus rekindled and reinforced by the realization of how little we seem to know about burnout even in "normal" (where vapor can easily escape) boiling (Lienhard, 1994; Sadasivan et al., 1995), I am back to my early fascination with nucleation, bubble growth, and associated micro layer phenomena. I neglected it then, but I hope now to find out how bubbles nucleate in superheated liquids by a slight motion that makes two solid interfaces touch. I outlined basic multiscale considerations then (Theofanous, 1980), but in this "nano" and "digital" age they seem finally to have come within reach. I hope in this paper to open a new window for direct observation and therefore create a new opportunity for finally understanding "burnout" in pool boiling — a truly basic subject with immense practical significance. In the words of John Lienhard (Lienhard, 1994) "we are back to Aristotle", but this time robustly so by seeing the real thing.

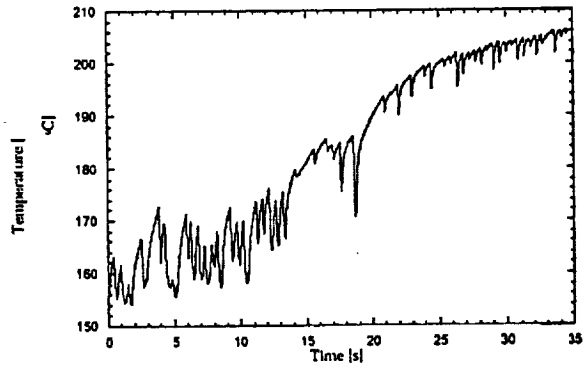

Figure 1: *Temperature mesurement on the ULPU downward facing heater during a burnout event.*

As mentioned already, in the downward facing geometry, we could see the real thing because the bubbles coalesced into a very thick (up to 10 cm) vapor film. By constraining the curved boundary within two flat vertical walls, and placing windows near the line of junction with the heater, we could observe, directly, the heater surface from within the vapor space (as soon as the liquid-vapor interface moved past the window). We had a periodic behavior, as the vapor film grew into a big, lens-shaped bubbled, gained buoyancy, and

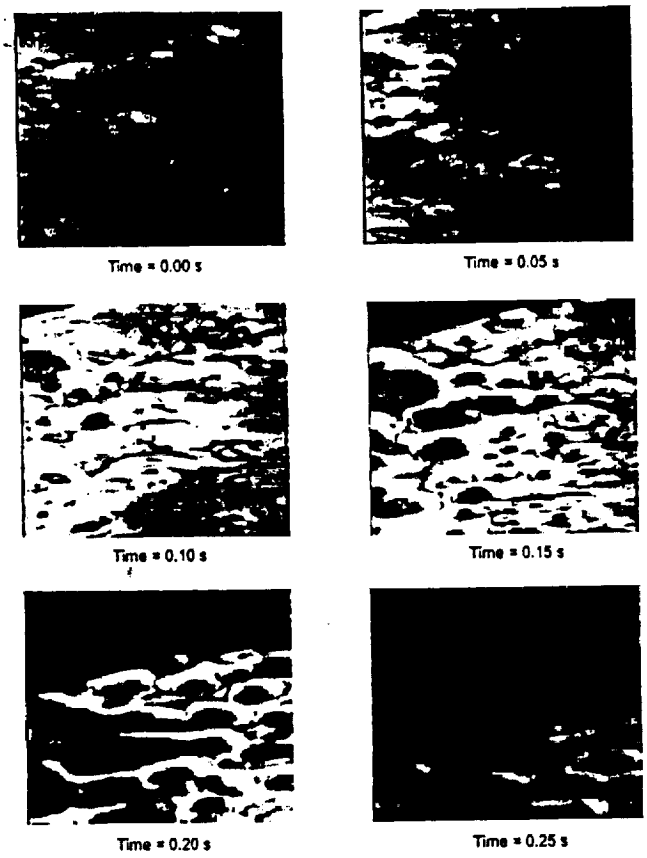

Figure 2: *Dry-out on a downward facing heater (mini-ULPU experiment).*

departed (slipping along the walls), allowing fresh water from below to contact the heater surface, and the beginning of a new cycle. The period increased slowly with heat flux and reached $\sim$ 500 ms at the limit of coolability. Cooling continued efficiently during this period by vaporization of a thin liquid layer left behind as bubbles coalesced to form the vapor film, very soon after they first nucleated. Early in the cycle the liquid layer continued to be disrupted by nucleation events and associated local microsprays. At the limit of coolability ($\sim$ 600 kW/m^2) such events produced leftover microcraters that grew in time revealing the solid surface beneath, and eventually merging to produce a large scale complete dryout within one period. A clear boiling crisis phenomenon was evident, but physical burnout was prevented because of the very large thermal mass of the heater. The result was a gradual heatup with superposed adiabatic excursions interrupted by periodic "quenches", as illustrated in Fig. 1 (Angelini et al., 1997). We reproduced this process in a separate, small experiment, with a flat heater of 5 cm in diameter, made to periodically touch the surface of a saturated water pool at controlled frequencies; that is, a process where the frame of reference is placed on the lower liquid-vapor interface of the "lens" produced in the big experiment. In this experiment, we could reach 800 kW/m^2 by increasing the frequency to 2.2 Hz, which was the limit conveniently achievable with the apparatus as designed (Theofanous et al. 1998). More importantly, with the new configuration we could observe more easily and in greater detail the dryout phenomenon just described, and a typical sequence of frames is shown in Fig. 2 (Theofanous et al., 1998). This shows remarkable similarities to the processes occurring in upward facing heaters during burnout, as we will see further below.

The difficulty with "normal" pool boiling is that even at fluxes as low as 20% of burnout the liquid vapor interfaces are so convoluted that it is it impossible to "see" anything; Lienhard (Lienhard, 1994) is quoting Chang's remark, "I have dreamed of bubbles, but I have never seen bubbles", after showing him strobe-frozen bubbles in a new boiling experiment he was building at Berkeley nearly 50 years ago. Lienhard takes this to emphasize the "eyes of the mind" and notes "This did not seem to be a place where he [Chang] would expect new truths to reveal themselves to him." To take this a little further, Chang's insight remaining true today, he seemed to know how hard it would prove to see the "bubbles that matter in boiling". Or perhaps having just suggested a hydrodynamics-based theory of boiling, this was Chang's polite negation of the very existence of bubbles (Chang, 1957). In fact, Bonilla and coworkers (Bonilla and Perry, 1941; Cichelli and Bonilla, 1945) had already correlated critical heat flux data on this basis, and then came Kutateladze (Kutateladze, 1948) and Zuber (Zuber, 1959) to lay claim to a complete, first-principles-based theory that had nothing to do with bubbles. With the appearance of the Haramura and Katto (1983) and the Dhir and Liaw (1989) models, we have completely different physical interpretations, still not direct observations, and yes, still not bubbles. The confusion is well described by Sadasivan et al. (1995), who call for significant new experimental efforts, and it is rendered in philosophical and poetic twists in a very enjoyable lecture by Lienhard (1994).

As described above, we delved into this work by a strong interest to "see", and our luck of having been able to do so in an inverted geometry. Our initial and basic step was to try to "see" from below, and our approach consisted of combining nano-scale heaters with high speed, high resolution infrared imaging. With the information so obtained we could identify a separation of scales that afforded us a simultaneous view of the key processes both from above (optical, high speed, high resolution) and from below. Lastly, we examined nucleation processes relative to heater morphology and aging at the nano-scale, using special experimental techniques and a battery of diagnostic procedures, including the Atomic Force Microscope (AFM). This last connection brings us to molecular dynamics as a whole new approach to looking at nucleation. The work is ongoing, and in the spirit of a keynote lecture, our aim here is to open a window, rather than to close a door.

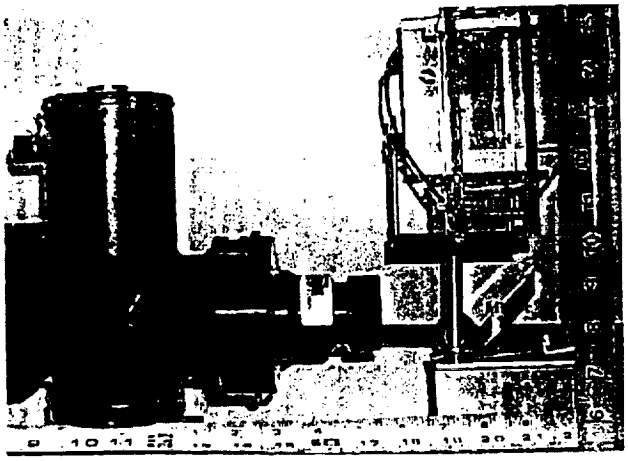

Figure 3: *The setup of the BETA experiment. Not shown are the video camera, associated lighting and the condensor on top of the vessel.*

2 The BETA Experiment

As indicated above, here we concentrate on saturated pool boiling on horizontal upward-facing heaters, and we are interested in the fundamental, direct, identification of the boiling crisis phenomenon. We wished to eliminate end effects (infinite flat plate behavior), and this we were able to achieve on a 20 x 40 mm heater, as demonstrated below. We wished to minimize, if not eliminate, heater thermal capacity effects, and this we achieved by means of a 140 nm titanium heater vapor-deposited on a 0.13 μm glass. We wished to start with a cavity-free heater surface, and this we achieved with a vapor deposition process that allowed an rms roughness of only $\pm$ 4 nm (as determined by AFM), very uniform, and very reproducible. The test vessel was made with optical quality Pyrex glass, and heating was provided by passing alternating current at controlled voltages. The power supply also allowed a choice of applied voltage, waveform, and frequency. In particular, with a square wave, a constant power situation could be obtained. The heater manufacturing required considerable development before spurious failures could be avoided, and true boiling crisis failures could be obtained (with water as coolant) at the requisite power levels of up to 1.2 MW/m^2.

A key point of this experiment is that the whole thermal pattern on the heater can be simultaneously visualized using high speed infrared thermometry. At 1157 frames per second, the focal plane consists of pixels which, applied to the whole heating surface, allows a resolution of 250 μm x 250 μm. On a closer close up, we focused on half the heating surface for a resolution of 156 μm x 156 μm. At 2083 frames per second, we could observe half of the heater at 156 μm x 156 μm resolution. A gold-coated mirror and special IR optics are used in the arrangement. Much higher spatial resolutions are possible with additional lenses, and a Sapphire substrate could improve further the transmission characteristics. The calibrations in the present experiments allow an accuracy of $\pm$ 2 K, but this can be improved to $\pm$ 0.5 K if desirable.

The whole experimental arrangement is shown in Fig. 3. At right angles to the IR camera, is a Kodak digital video camera (not shown) with capability of up to 10,000 frames per second at resolution of 34 x 128 pixels. The two cameras can be synchronized.

The heater surface morphology was characterized by means of four different techniques. First, the overall view is obtained by means of a standard optical microscope (OM1) at a magnification of x1000. Then, any special features, such as protuberances, are examined with a very small depth of field optical microscope equipped with a Nomarski prism (OM2). Quantitative local detail was obtained with an Atomic Force Microscope (AFM). Finally, any local features larger than a few hundred nanometers were imaged with a Scanning Electron Microscope (SEM). The detailed implementation of these techniques to the particulars of the BETA experiment, including local chemical characterization with the SEM (ion mass spectroscopy), are still under development.

As a counterpart to this extreme care in heater characterization, we have also developed special cleaning and handling techniques for the fluids (up to now only water) throughout the process — from heater installation, to running an experiment, removing a heater, and handling for detailed examination. In particular, we could demonstrate by direct comparison that we could carry out this complete process for an experimental run taken all the way to burnout without affecting any aspect of the morphology whatsoever. Our "natural aging" processes are not as precise yet, but as described below, these first results are so interesting as to demand extensive continuing study, both experimentally and theoretically. Indeed, one of our major conclusions is that mesoscale-level processes on the heater surface control everything. Further, we show that these can be controlled to a sufficient degree so as to be predictable, and of value in real engineering applications.

3 Experimental Results and Discussion

The experimental program conducted so far is summarized in Table 1. As indicated, our heaters proved remarkably resistant to burnout. We can see that with aged heaters we essentially reached ($\sim$ 90%) the so-called hydrodynamic (Kutateladze–Zuber, K–Z) limit, while even the fresh heaters allowed as much as 75% of it. By comparison, Golobic and Bergles (1992) correlation based on their $\delta(\rho ck)^{0.5}$ parameter yields 50 to 60% depending on whether we used the heater only or the heater-glass composite properties respectively. Also interesting is the comparison with the data of Guglielmini and Nannei (1976), obtained with 400 nm heaters that yielded CHF values of only $\sim$20 % relative

Table 1: *BETA Experiments with Titanium nanofilm heaters.*

Heater	*Heater condition*	*Water coolant*	*Wetting angle*	*AC Power Freq. (Wave form)*	*Test conduct*	*CHF** $(\frac{kW}{m^2})$	*CHF**max* $(\frac{kW}{m^2})$
A	Fresh	Distilled	-	60 Hz (sin)	Multiple runs before CHF	669	1338
B	Fresh	Distilled	-	60 Hz (sin)	Multiple runs before CHF	619	1238
D	Fresh	Distilled	45° [a]	60 Hz (sin)	Single run to CHF	600	1200
F	Aged	Aged Distilled	-	60 Hz (sin)	Multiple runs before CHF	1159	2308
G	Aged	Aged Distilled	20° [b]	1000 Hz (sin)	Multiple runs before CHF	1062	2124
H	Aged	Aged Distilled	-	1000 Hz (sin)	Multiple runs before CHF	1185	2370
I	Cleaned after aging	Chemically clean	-	30 Hz (square)	Single run after cleaning of the heater	885	885
J	Fresh	Chemically clean	-	30 Hz (square)	Single run to 879 $\frac{kW}{m^2}$	879+	879+
K	Fresh	Chemically clean Degassed	55° [c]	30 Hz (square)	Single run to CHF	934	934

[a] - Typical for A-E heaters.
[b] - Typical for F-H heaters.
[c] - Typical for J-K heaters.
+ - Taken to Burnout by coolant depletion, after achieving 879 kW/m^2 at steady state.
* - Mean value as measured by an rms voltmeter, and ampermeter.
** - Peak heat flux on waveform.

to the K–Z limit. Further on this table we show the effect of time-at-power on CHF as caused by the sinus-shaped voltage waveforms. The 60 Hz runs yield ms-scale time frames at the peak powers shown by the last column on the table. It is seen that the fresh heaters (A, B, D) reach the K–Z limit, but we believe that this is a coincidence. On the other hand, the aged heater (F), operating at 60 Hz reached 2308 kW/m^2. The 1000 Hz runs yielded tens of μs-scale time frames at peak power, and they could withstand over 2 MW/m^2; however, at such time frames it may well be that the transient response is sufficiently smoothed so that the peak values are not really relevant. A resistance to burnout with decreasing the time-at-power is thereby evident. While in general not unexpected, the quantitative aspects of this behavior could prove very valuable in elucidating the basic mechanisms. For example, in the 60 Hz runs, we could obtain a much more pronounced "hot-spot" behavior, to be discussed shortly.

From the critical heat flux trend, all of our experiments can be put into two main categories of behavior, heater aging being the principal parameter. This is also reflected in the heater temperature patterns observed, and both appear to be the immediate consequence of the nucleation characteristics. Within the fresh (or cleaned) heater category there is the time-at-power effect just discussed. However, this effect is only quantitative, and the basic behavior as revealed by the heater temperature patterns is very similar. Keeping this in mind, and as a consequence of the space limitations, here we provide further details only for heaters G and K.

Sample frames of the IR movies that show the variations of temperature patterns with heat flux and heater morphology are shown in Figs. 4 and 5 (heaters G and K respectively). Each dark spot on these figures indicates the enhanced cooling due to microlayer evaporation at the base of the vapor bubbles. Comparison between the two figures therefore indicates drastically different nucleation characteristics. Also remarkable is the uniformity achieved at high heat fluxes. In concomitance to a lower number density, the fresh heater is characterized with much larger "bubbles". This is consistent with the larger liquid superheats (light region in Fig.5b) and this in turn is consistent with the larger mean distance between the enhanced-cooling regions.

Recognizing the spatial uniformity of applied power, and the highly curtailed potential for radial diffusion (ultra-thin heater, thin and poorly conducting glass substrate), we can convert these images to microlayer thickness maps. Thus, for Fig. 4c we find that the whole surface is covered with a microlayer varying in thickness between 10 and 25 μm. Similarly, for Fig. 5c, we have 7 and 30 μm. The large bright spot in the left-middle of Fig. 5c is the dryout region developed at the early stages of burnout. On the other hand, the spreading of the burnout zone with time is shown in Figs. 6 and 7.

From the IR movies we can deduce that all dark spots behave in a dynamic manner, but some only oscillate in size and slightly in temperature, while others disappear completely to reappear a little later at the same location (Fig. 8). These of the latter kind develop to larger sizes, and when close to burnout fluxes within them develop short-lived "hot spots," as illustrated in Figs. 8 and 9. These figures were extracted from movies that image the whole heater surface. Much better spatial resolutions are possible by focusing the camera to a position of the heater with size corresponding to just a few nucleation sites. For fresh heaters, burnout seems to originate in such hot spots. A typical temperature history at the hot spot location is show in in Fig.10, where crosses correspond to IR images shown in Fig.9. Hot spots could also be seen in the case of aged heaters, but they were of much reduced size (note the much smaller size of the cool spots themselves and frequency), and so far we have not succeeded in catching them in the act of causing burnout. In any case, the regularity of this behavior indicates that each dark spot is a consequence of a single nucleation event, and that the hot spots develop precisely at the point of nucleation. Further, given the estimates provided in the previous paragraph, it appears that these nucleation events, for power levels near burnout, occur within a liquid microlayer of a few tens of microns in thickness. In some cases it may be that the crater thus formed remains open, while in other cases it appears to close by either spreading from the nearby thicker-film regions, or by liquid drops raining down from above. Thus we are reminded of the downward facing geometry shown in Fig. 2.

This picture is consistent with the very high void fraction ($\sim$ 90%) known to exist at power levels close to burnout, in the immediate vicinity of the heater (300 to 1000 μm). Also, at such power levels ($\sim$ 1 MW/m^2) we would need only one 2-mm liquid drop per square centimeter per 100 ms to supply the water make up for the amount vaporized. It appears that the liquid is lifted by vapor bubbles sufficiently to allow heat removal by microlayer evaporation throughout the surface of the heater, while at the same time, liquid supply from above cannot impose any limitation. To further bolster that, we note that the superficial vapor velocity is below 1 m/s, while the vapor velocity needed to lift a mm-sized drop is over 10 m/s.

Thus we come to conclude that burnout is not hydrodynamically limited (in the K–Z sense), and that it is strongly affected by bubble nucleation processes within a microlayer that covers the heater surface macroscopically, but it has microscopic (tens of microns) and highly dynamic local behavior. It is the rupture of this microlayer that is responsible for burnout, and this process appears to be highly regular, in that it could be seen to originate very nearly simultaneously on several spots of the heater. Also, it appears to be higher reproducible. Beyond nucleation, also important in

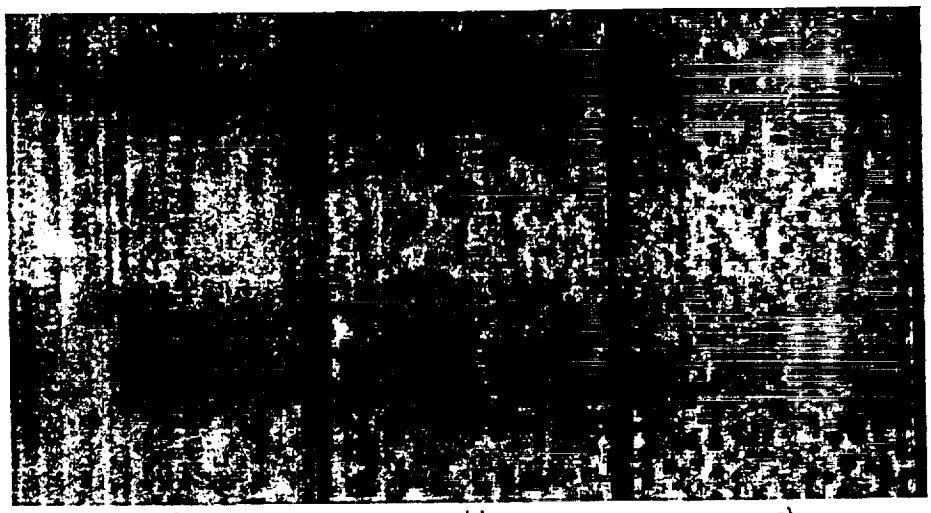

Figure 4: *IR images for test runs of Series G. Heat fluxes $q'' = 116$ (a), 620 (b) and 1062 (c) kW/m^2.*

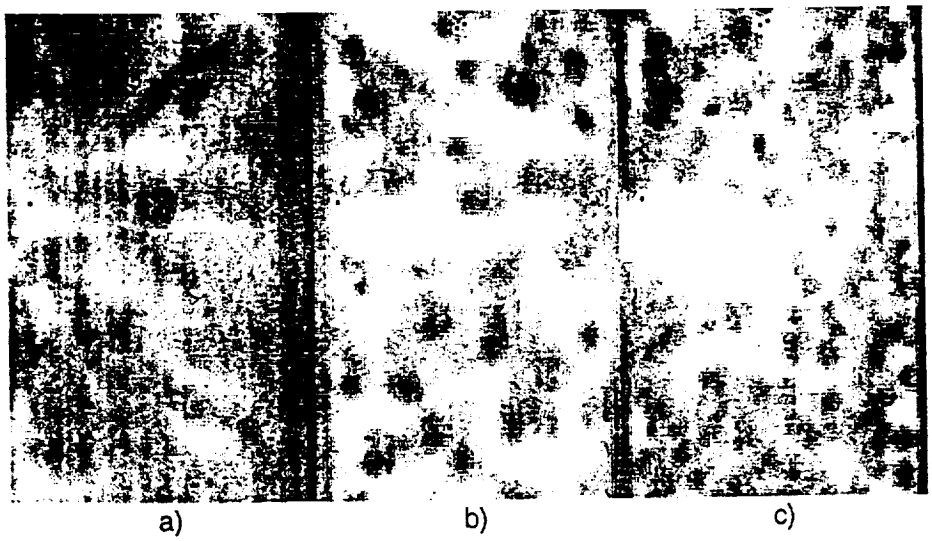

Figure 5: *IR images for test runs of Series K. Heat fluxes $q'' = 76$ (a), 612 (b) and 934 (c) kW/m^2.*

this respect is the growth of vapor bubbles within such microlayers, as well as the detail manifestation of the microlayer-disruption processes that follows.

To further demonstrate this, we ran heater J by allowing, at the end, the coolant to deplete after bringing it very close to the burnout heat flux. Indeed, we found the behavior to remain unchanged until a very thin liquid film began to dry out, leading to the spreading of very high temperature regions. The heater survived long enough to resolve this spreading phenomenon and record the coexistence with the very effectively cooled regions covered by a microlayer–bubble nucleating within it still being visible (see Fig. 7). Again, this is reminiscent of what was observed in Fig. 2, and this is remarkable given the huge differences between the two systems.

Lastly, we come to relate heater surface characteristics to nucleation and dryout behavior. First, for heater K the OM1 shows no difference before or after the run. We could see a very smooth surface, uniformly speckled with bright spots 2-3 μm in diameter, to a density of $\sim 100/\text{cm}^2$. The SEM shows these to be protrusions, rather than cavities. The AFM measurements reveal that outside of these protrusions the surface is very smooth with a regular roughness of $\sim$ 5 nm rms (see Fig. 11). Still the superheats did not exceed 40 K. We believe that heterogeneous nucleation deserves a new look (including the nucleation behavior mentioned in the introduction), taking into account the nanoscale features and molecular interactions at a superheated surface, and we are pursuing such investigations using methods of molecular dynamics. In this light the wetting contact angle previously used to characterize boiling would appear to be too crude a measure, and this is bolstered by our aged-heater data. Here, OM1 shows a very rough surface, full of protrusions, rounded at the base, and up to 10 μm in diameter. OM2 shows that the height of these protrusions

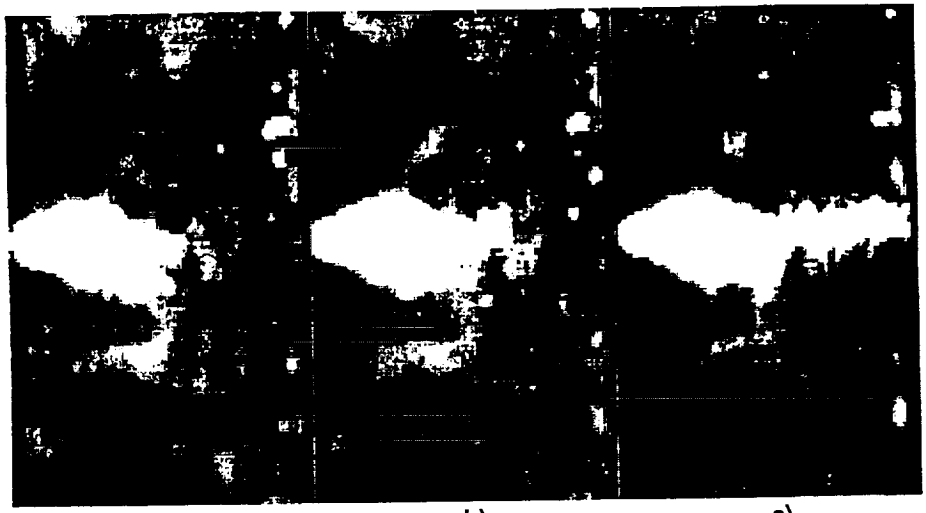

Figure 6: *Burnout sequence in a pool boiling at 934 kW/m^2 (K heater). Time interval 30 ms.*

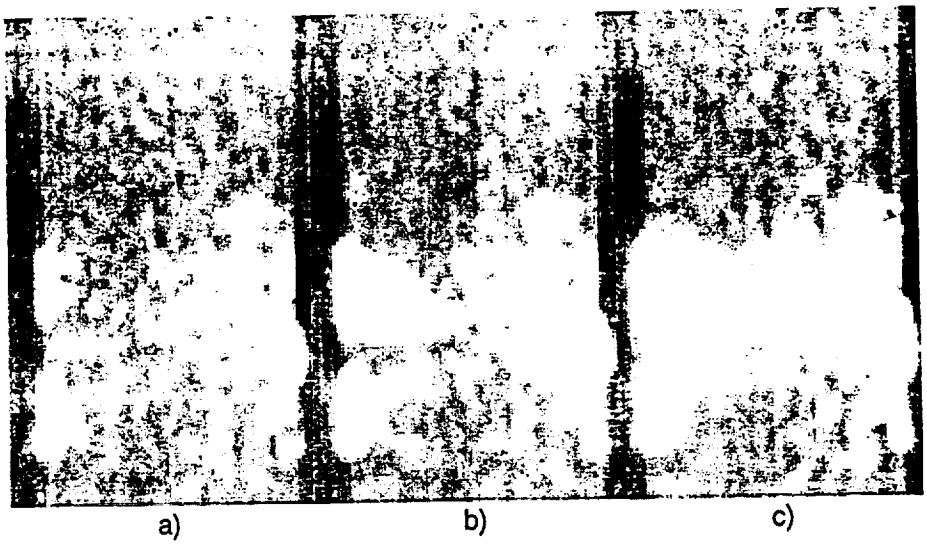

Figure 7: *J burnout sequence. Time interval 100 ms.*

is up to a few microns. AFM measurement at spots in between these protrusions shows height variations of up to 50 nm, with an rms value of ~20 nm. Further, the spatial pattern of these AFM measurements reveal a "wick-like" structure. In this light it is not hard to understand the nucleation behavior (Fig. 4), and the resistance to dryout by wicking (heat-pipe-like) action. This microcosm is clearly much more complicated than that of "fresh" heaters, and now it is important to understand how this complexity arises, in addition to its effects on nucleation and capillary motions. Systematic variations in "exposure," and painstaking observations would be required for this purpose. Also, simultaneously to normal boiling configuration, the depletion and downward facing experiments discussed here could play a significant role in this quest.

4 Concluding Remarks

A new diagnostic technique, together with the identification of a separation of scales, have allowed us a unique opportunity to probe directly into the basic mechanisms of burnout in saturated pool boiling. This brings out the importance of nanoscale morphology of the heater surface, and perhaps the chemistry of the solid-liquid pair, on nucleation processes and the behavior of micron-scale liquid films, all being wide-open areas for investigation. Further, this opens up new possibilities for a unified study and coherent treatment of microgravity (we are preparing fluid drop tower testing at NASA Lewis), multicomponent behaviors, and ultimately convective and subcooled boiling. There is also an immediate practical significance of our results in that we have been able to manufacture ultrathin heaters capable of dissipating powers at an excess of 1 MW/m^2 at steady state.

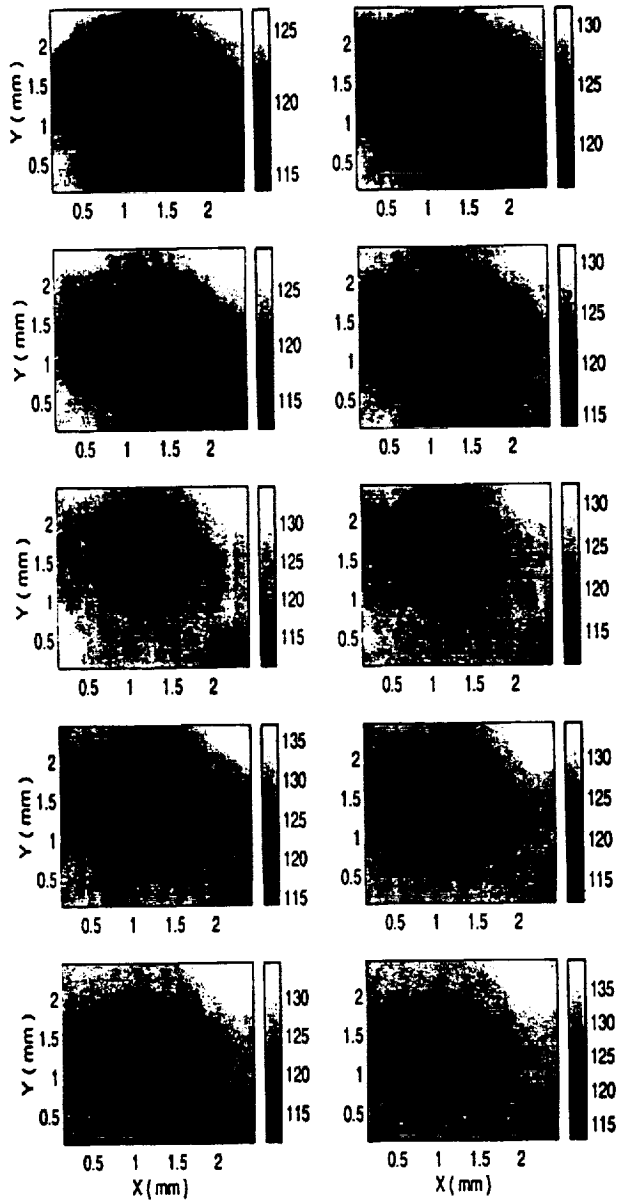

Figure 8: *IR images of large bubbles at a fixed location (A run, $q" = 635\ kW/m^2$). Time interval between pictures is 30 ms.*

5 Acknowledgement

This work began under DOE's ARSAP program a few years ago, and it is presently pursued under NASA Grant NAG3-2119 cooperatively with US Nuclear Regulatory Commission Contract NRC-04-98-051.

References

1. Angelini S.,Buyevich Y. and Theofanous T.G. (1997) The mechanism and prediction of critical heat flux in inverted geometries, NURETH-8, Kyoto Japan, September 30-October 4 v. 1, 147-156.

2. Bonilla C.F. and Perry C.W. (1941) Heat transmission to boiling binary liquid mixtures, Trans. A.I.Ch.E., v. 37, pp. 269-290.

3. Chang Y.p. (1957) A theoretical analysis of heat transfer in natural convection and in boiling, Trans. ASME, v. 79, p. 1501.

4. Cichelli M.T. and Bonilla C.F. (1945) Heat transfer to liquids boiling under pressure, Trans. A.I.Ch.E., v. 41, p. 755.

5. Dhir V.K. and Liaw S.P. (1989) Framework for a unified model for nucleate and transition pool boiling, J. Heat Transfer 111, 739-45.

6. Golobic I. and Bergles A.E. (1992) Effects of thermal properties and thickness of horizontal

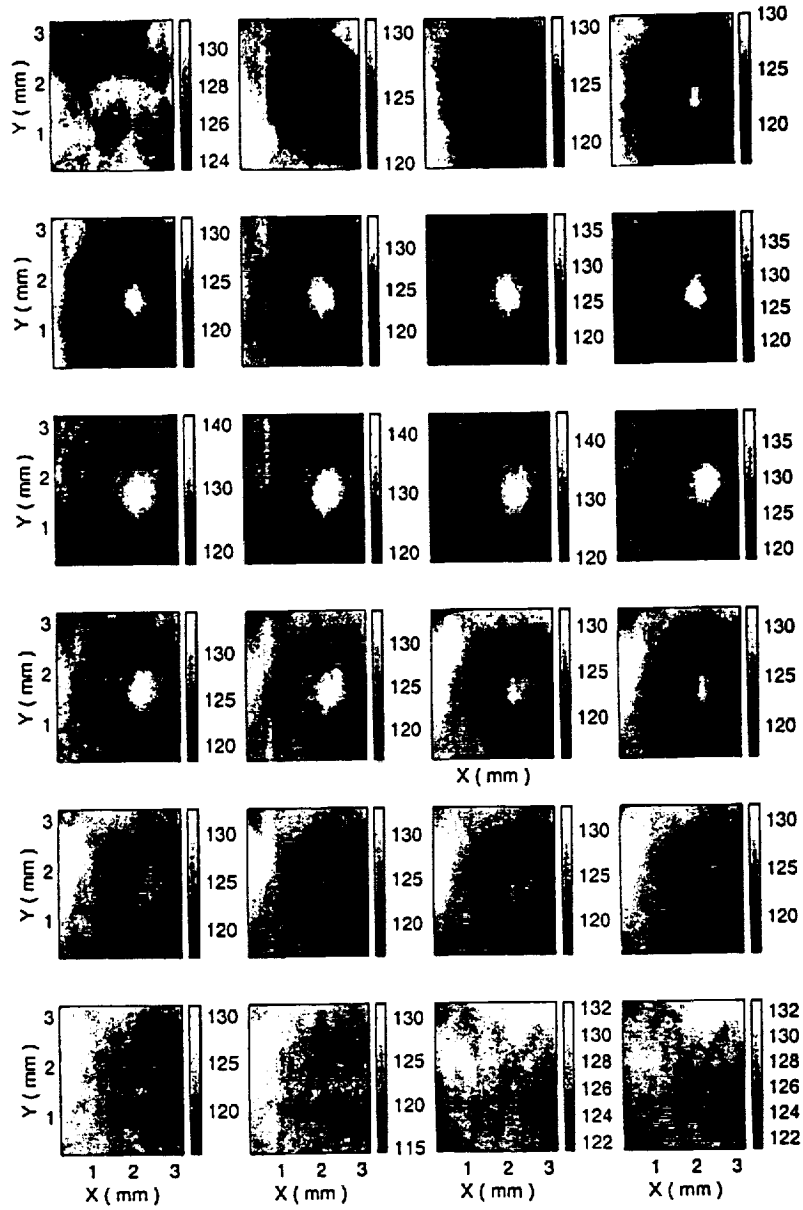

Figure 9: *Dynamic thermal footprint of a large bubble with formation of hot spot (K run, $q" = 830\ kW/m^2$). Time interval between pictures is 2 ms.*

vertically oriented ribbon heaters on the pool boiling critical heat flux, Proceeding of Engineering Conference on Pool and External Boiling, March 22-27, Santa Barbara, USA.

7. Guglielmini G. and Nannei E. (1976) On the effect of heating wall thickness on pool boiling burnout, Int. J. Heat Mass Transfer, vol. 19, p. 1073.

8. Haramura Y. and Katto Y. (1983) A new hydrodynamic model of critical heat flux, applicable widely to both pool and forced convection boiling on submerged bodies in saturated liquids, Int. J. Heat Mass Transfer, v. 26 No. 3, pp. 389-399.

9. Lienhard J.H. (1994) Snares of pool boiling research: putting our history to use. Lecture

10. Kutateladze S.S. (1948) On the transition to film boiling under natural convection, Kotloturbostrenie, No. 3, p. 10.

11. Sadasivan P., Unal C. and Nelson R. (1995) Perspective: issues in CHF modeling—the need for new experiments, Trans. ASME, J. Heat Transfer, v. 117, 558-567

12. Theofanous T.G. (1980) The boiling crisis in nuclear reactor safety and performance, Int. J. Multiphase Flow, 6, 69-95.

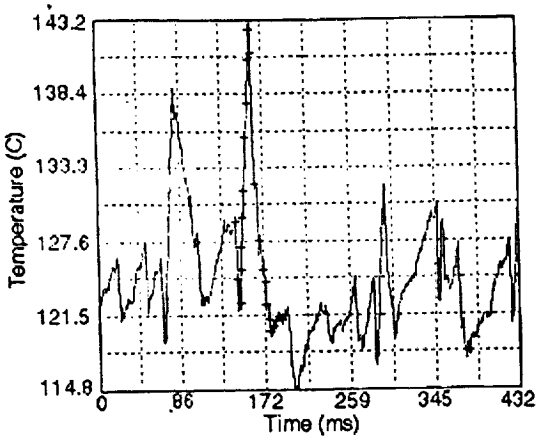

Figure 10: *Temperature history at the hot spot location. Crosses correspond to IR images in Fig.9*

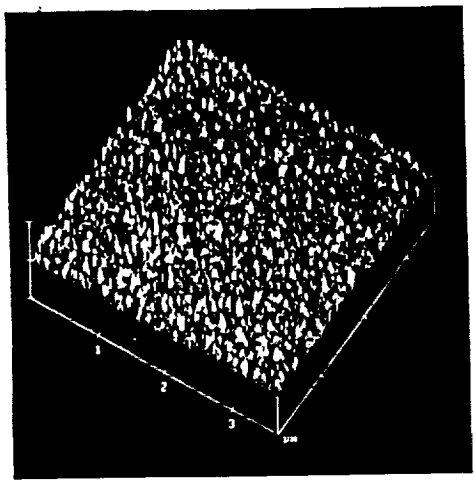

Figure 11: *AFM image of a 3 μ m x 3 μ m region on heater K after burnout. The vertical scale is 15 nm/division.*

13. Theofanous T.G. and Patel P.D. (1976) Universal relations for bubble growth, Int. J. Heat and Mass Transfer, 19, 425-429.

14. Theofanous T.G., Bohrer T.H., Chang M.C. and Patel P.D. (1978) Experiments and universal growth relations for vapor bubbles with microlayers, J. Heat Transfer (ASME), 100, No. 1, 41-48.

15. Theofanous T.G., Liu C, Additon S., Angelini S., Kymäläinen O. and Salmassi T (1996) In-Vessel Coolability and Retention of a Core Melt, DOE/ID-10460, Vols. 1 and 2, October and Nucl. Engr & Design, 169 (1997) 1–48.

16. Theofanous T.G. and Syri S. (1997) The coolability limits of a reactor pressure vessel lower head, Nucl. Eng. and Design, 169, 59-76.

17. Theofanous T.G., Tu J.P., Mäepää T.K., (1998) The mechanism and prediction of critical heat flux in inverted geometry, 3rd International Conference on Multiphase Flow, June 8–12, Lyon, France.

18. Zuber N (1959) Hydrodynamic Aspects of Boiling Heat Transfer, Ph.D. thesis, UCLA, Los Angeles, (Also available as AECU-4439 Physics and Mathematics.)